1

3D/4D Printing in Additive Manufacturing: Process Engineering and Novel Excipients

Christian Muehlenfeld[1] *and Simon A. Roberts*[2]

[1] *Ashland Industries Deutschland GmbH, Paul-Thomas-Straße 56, 40599 Düsseldorf, Germany*
[2] *Ashland Specialties UK Ltd., Vale Industrial Estate, Stourport Road, Kidderminster, Worcestershire, DY11 7QU, UK*

1.1 Introduction

In recent years, additive manufacturing, which is more colloquially referred to as three-dimensional (3D) printing, has seen high-impact implementation in manufacturing applications in areas such as aeronautics, robotics, electronics, industrial goods, and even the food industry. These wide-ranging applications have resulted in a change in focus for biomedical research [1]. 3D printing is a generic term that describes various methods of constructing objects in a layer-by-layer manner. Although the birth of 3D printing dates back to 1984, when Charles Hull invented the first stereolithographic printer, 3D printing started to increasingly change the way in which manufacturing was performed from the year 2000 onward.

This chapter will introduce the basic concepts of 3D and 4D printing technologies as they pertain to biomedical applications. In particular, 4D printing (printing of objects with the ability to change over time) has a strong potential for biomedical applications. Patient-specific products such as medical devices, tissue constructs (including muscle structures, bone, and ear tissue), and, eventually, artificial organs may be fabricated using 4D printing [2–6].

1.2 The Process of 3D and 4D Printing Technology

3D printing typically begins with a computer-aided design (CAD) file that describes the geometry and size of the objects to be printed. The object is sliced into a series of digital cross-sectional layers that are then fabricated by the 3D printer. This process can use many different types of materials such as thermoplastic polymers, powders, metals, and ultraviolet (UV) curable resins.

Four-dimensional (4D) printing is defined as printing of 3D objects with the ability to change the form or function under the influence of external stimuli over time [7, 8]. A schematic of printing dimensions is shown in Figure 1.1.

3D and 4D Printing in Biomedical Applications: Process Engineering and Additive Manufacturing,
First Edition. Edited by Mohammed Maniruzzaman.

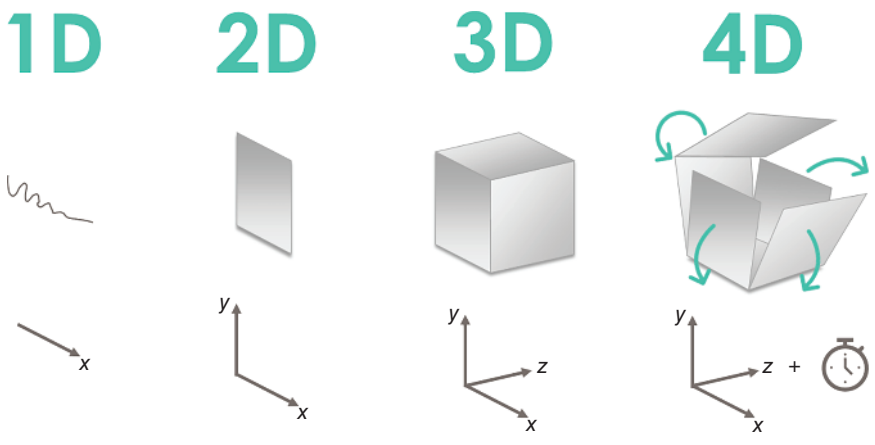

Figure 1.1 Schematic of 1D, 2D, 3D, and 4D printing dimensions. In a 4D system, a 3D printed object undergoes time-dependent deformations when exposed to various stimuli.

The essential difference between 4D printing and 3D printing is the addition of smart design, or responsive materials, that results in a time-dependent deformation of the object. In order to achieve this goal, the printed material needs to self-transform in form or function when exposed to an external stimulus such as osmotic pressure, heat, current, ultraviolet light, or another energy source [9]. Incorporating these additional functions poses major challenges to the design process because 4D printed structures must be preprogrammed in detail, based on the transforming mechanism of controllable smart materials that incorporate the requested material deformations. Because most 3D printing materials are designed only to produce rigid, static objects, the choice of materials for 4D printing is significant.

1.3 3D/4D Printing for Biomedical Applications

3D and 4D printing technologies have the potential for great impact in biomedical applications. 3D printing allows printing of biomaterials as well as living cells to build complex tissues and organs, whereas 4D bioprinting is an extension of the process that adds additional value. Different approaches can be used for 4D printing of biomaterials. The first approach strictly follows the original concept of 4D printing, in which a substrate material folds into a predefined 3D configuration upon stimulus. The printed cell or tissue material is incorporated within the device during printing and subsequently follows the folding of the substrate as it forms into a desired shape postimplantation.

The second approach is based on the maturation of engineered tissue constructs after printing and could be considered as a kind of *in vivo* 4D bioprinting. A 3D printed polymer medical device is implanted first and then accommodates the growth of tissue or organ over the postsurgical period.

1.4 Smart or Responsive Materials for 4D Biomedical Printing

The 3D and 4D printing technologies are classified mainly based on the types of materials used. The selection of materials has a direct influence on mechanical or thermal properties, as well as the transformation stimuli of the finished objects. Although the major difference between 3D and 4D printing is in the materials, the processes used to fabricate printed objects are the same. It should be pointed out that 4D printing is still in its early development stage. Herein, some example applications are presented to demonstrate its potential.

Although numerous materials are available for 3D printing, currently, limited stimuli-responsive biomaterials are available for 4D printing. At present, researchers are focused on the development of various, novel, smart materials; however, not every smart material can be 3D printed. The most common materials used in 4D printing are biocompatible materials such as hydrogels and polymers. Table 1.1 lists some examples of smart biomaterials intended for biomedical applications based on their stimulus responsiveness. Some of them have already been used for 4D printing, but it is unclear whether others of these materials can be used in 3D/4D printing in the future. The mechanisms facilitating 4D temporal shape transformation of 3D printed materials for biomedical applications range from temperature responsiveness, magnetic field responsiveness, and light responsiveness to humidity responsiveness.

A simple mechanism facilitating 4D shape transformation of 3D printed materials is the shape memory properties of thermoresponsive materials. Poly(*N*-isopropylacrylamide) (pNIPAM) hydrogels are well-known examples, in which the transformation principle is based on the wettability and solubility alteration of the thermoresponsive hydrogel following a change in temperature. Figure 1.2A shows an example of a photo-crosslinked, acrylic acid-functionalized pNIPAM (pNIPAM-AAc) in combination with polypropylene fumarate, where the pNIPAM-AAc component is transformed to a hydrophobic state showing shape transformation after increasing the temperature above 36 °C [10]. Zarek et al. [11] presented a strategy to capitalize on a series of medical imaging modalities to construct a printable shape memory endoluminal device, exemplified by a 4D printed tracheal stent made from methacrylated poly(ε-caprolactone) (PCL) that can be deformed into a temporary shape, inserted in the body, and then deployed back into its permanent shape with a local increase in temperature. Huang et al. [12] used biodegradable poly(L-lactic acid) (PLA) surgical staples as an alternative to biodegradable sutures in minimally invasive surgery for wound closure. Those staples are used in a stretched form and show a self-tightening function upon heating to slightly above body temperature (about 45 °C, which is within the glass transition temperature range of PLA) (Figure 1.2B). Another example based on the concept of temperature responsiveness is a poly(vinyl alcohol) (PVA)–poly(ethylene glycol) (PEG) double-network hydrogel, which was able to transform back from a stabilized helix structure after 15 seconds of immersion in hot water (90 °C), causing molten crystalline domains of PVA and

Table 1.1 Examples of smart or responsive materils suitable for biomedical purposes.

Stimulus	Material type or name	Composition and remarks	Print process	References
Temperature	pNIPAM-AAc	Poly(*N*-isopropylacrylamide-co-acrylic acid) (pNIPAM-AAc), polypropylene fumarate (PPF), iron oxide (Fe_2O_3) nanoparticles	—	[10]
	Methacrylated polycaprolactone	Poly(ε-caprolactone) (PCL) dimethylacrylate, 2,4,6-trimethylbenzoyl-diphenylphosphineoxide (TPO) as photoinitiator, vitamin E to prevent premature cross-linking, Toner Yellow 3GP	SLA (Freeform pico 2 SLA digital light processing printer)	[11]
	PLA surgical staples	Poly(L-lactic acid) (PLA)	Not mentioned	[12]
	PVA/PEG hydrogel	Poly(vinyl alcohol) (PVA)–poly(ethyleneglycol) (PEG) double-network hydrogel	—	[13]
	Soybean-oil-epoxidized acrylate liquid resin	Soybean-oil-epoxidized acrylate contains three major fatty acid residues (stearic, oleic, and linoleic acid) with pendant alkane groups that may freeze and benefit shape fixing at −18 °C.	SLA (modified Solidoodle® 3D printer platform)	[14]
Magnetic field	PEGDA/PHEMA soft microrobot	PEG acrylate (PEGDA), iron (II, III) oxide (Fe_3O_4); 2-hydroxyethyl methacrylate (PHEMA) layer	—	[15]
	Macroporous ferrogel	Peptides containing the arginine–glycine–aspartic acid (RGD) amino acid sequence, sodium alginate, Fe_3O_4 nanoparticles	—	[16]
Light	Optogenetic muscle ring-powered biobots	PEG acrylate (PEGDA) photosensitive resin	SLA (SLA 250/50; 3D systems)	[5]
	PHEMA hydrogel	Cross-linked PHEMA, functionalized with azobenzene groups	—	[17]
Humidity	PCAD@AG	PEG-conjugated azobenzene derivative (PCAD) and agarose (AG)	—	[18]
	$CSE_{0.3}$	Cellulose stearoyl ester with low degree of substitution (DS = 0.3)	—	[19]
Osmotic pressure	PEG hydrogel	Photo-crosslinkable PEG with 1-[4-(2-hydroxy-ethoxy)-phenyl]-2-hydroxy-2-methyl-1-propane-1-one (Irgacure 2959) photoinitiator	—	[20]
	Vinyl caprolactam/PE hydrogel	Vinyl caprolactam, polyethylene, epoxy diacrylate oligomer, Irgacure 819	Stratasys Connex 500 Multi-Material 3D Printer	[21]

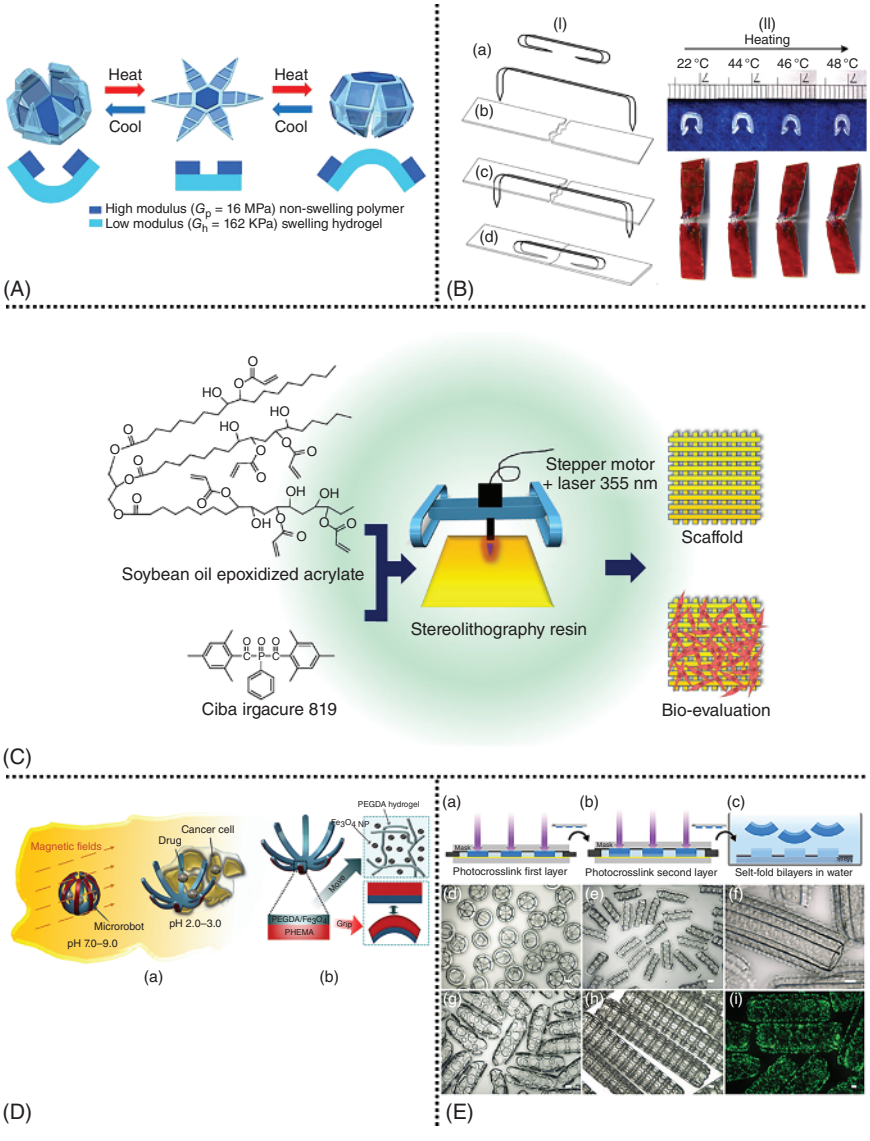

Figure 1.2 (A) Schematic diagram illustrating the reversible self-folding of soft microgrippers in response to temperature. Source: Breger et al. 2015 [10]. Reproduced with permission of ACS. (B) Self-tightening of a PLA staple. (I) Concept. (a) Original shape of a staple; (b) after programming; (c) after being fired into tissue; (d) after heating for tightening; (II) experimental result (Insorb® staple). Top: shrinking of staple upon heating; bottom: tightening of staple upon heating to bring two pieces of tissue closer. Source: Huang et al. 2013 [12]. Reproduced with permission of Elsevier. (C) Schematic of soybean-oil-epoxidized acrylate fabrication process from raw material through resin fabrication and application. Source: Miao et al. 2016 [14]. https://creativecommons.org/licenses/by/3.0/. (D) Schematic diagram illustrating the proposed soft microrobot, which can move freely by magnetic fields. Trapping and releasing of drug microbeads at the destination target by folding and unfolding motions is triggered by different pH values. Source: Hao et al. 2016 [15]. Reproduced with permission of IOP Publishing. (E) Schematic diagram illustrating the osmotic-pressure-driven deformation. Side view schematic of the three basic PEG bilayer photo-crosslinking steps (a–c) and examples of self-folded hydrogel geometries (d–i). (Source: Jamal et al. 2013 [20]. Reproduced with permission of John Wiley & Sons.)

thus transform back to a straight line [13]. Miao et al. [14] used the concept of thermoresponsiveness for biomedical scaffolds fabricated using a stereolithography (SLA) printer. Polymerized epoxidized soybean oil acrylate was used because of its thermoresponsive properties and glass transition temperature of approximately 20 °C, which could revert to its original shape at approximately 37 °C (Figure 1.2C).

Hydrogels containing magnetic particles, or ferrogels, are examples of magnetic-field-responsive materials. Figure 1.2D shows a 3D printed magnetic-field-responsive soft microrobot made of a poly(ethylene glycol) acrylate (PEGDA) and 2-hydroxyethyl methacrylate (PHEMA) hydrogel bilayer structure containing iron oxide particles (Fe_3O_4), which can move under an external magnetic field to the target site and release an encapsulated drug, triggered by a change in pH [15]. Another example is an alginate-based scaffold driving the outward movement of water from the internal pores under the influence of a magnetic field, thus triggering the release of cells or biological agents [16].

Light-responsive materials may convert their shape based on photoisomerization and photodegradation in the polymer chain. These mechanisms have been applied in artificial muscle biobots, where stereolithographic 3D printing was used to fabricate ring and strip injection molds and biobot skeletons from a PEGDA photosensitive resin [5]. Another example of light responsiveness is the use of cross-linked PHEMA functionalized with azobenzene groups, where light irradiation modifies the degree of swelling [17].

Humidity-responsive material uses include the humidity-induced bending of PEG-conjugated azobenzene derivatives with agarose (PCAD@AG) films [18], or cellulose-based materials [19].

An example of osmotic-pressure-driven hydrogels using intrinsic swelling characteristics was demonstrated using photo-crosslinkable PEG with varying molecular weights [20]. Printed as bilayered constructs with 1-[4-(2-hydroxyethoxy)-phenyl]-2-hydroxy-2-methyl-1-propane-1-one as the photoinitiator, differences in the swelling behavior of the hydrogel layers result in a shape transformation to form micropatterned structures (Figure 1.2E). This principle was adapted by adding a non-swelling but flexible material as the second layer to form joints between rigid linear structures [21].

However, all of these applications have been tested in biomechanically non-challenging environments. Therefore, direct biomedical application is currently restricted by material limitations and the complex host environment of the targeted tissue(s). Accordingly, not all stimuli may be applicable for use in biomedical applications. Although humidity responsiveness is widely present in nature, application of this stimulus could be restricted because of the limitations of humidity or osmotic pressure that can be applied to the constructs used for biomedical purposes. Taken together, these examples demonstrate that novel excipients and excipient combinations can be used to induce temporal shape transformation for 4D printing; however, performance has not been tested in biomechanically challenging environments. Thus, follow-up studies employing and characterizing these introduced concepts and, furthermore, using medical grade materials are necessary and important.

1.5 Classification of 3D and 4D Printing Technologies

Although a broad variety of technologies have been developed for industrial fabrication of 3D structures, there are only few major technologies used for biomedical printing. These include extrusion-based (fused filament), droplet-based (using chemical agents/binders), and laser-based systems (sintering/melting) to print the material. Each technique differs in the manner in which layers are built and printing materials are used (Figure 1.3). Furthermore, each of these shows certain process characteristics that might be preferable for different applications. The advantages and disadvantages associated with each approach can be demonstrated by comparing the dimensional accuracy, mechanical properties, surface roughness, build speed, and materials cost, across multiple 3D printing platforms [22]. A comprehensive summary of each technology is given in the following sections.

1.5.1 Fused Filament Fabrication (FFF) – Extrusion-Based Systems

Fused filament fabrication (FFF) is an extrusion-based printing technology, also known by the trademark name Fused Deposition Modeling™ (FDM)[23]. The FFF systems use solid filaments that are heated above the melting temperature of the material and then the extruded melt is deposited using a Cartesian coordinate robot in a continuous flow to build up a 3D printed part in a layer-by-layer manner. When each layer in the *xy* plane is finished, the platform (*z* axis) is lowered and the procedure is repeated (Figure 1.4). This process continues until the whole part is complete. Because of thermal fusion, the material bonds with the layer beneath and solidifies, thus forming a permanent bonding of the two layers. To improve the interlayer bonding, the entire process is performed in a closed chamber maintaining a constant temperature [24].

Multiple printheads can be accommodated in FFF devices, allowing the use of different materials within a single 3D printed object. If necessary, a second printhead is used to provide a temporary support substrate for complex structures with an overhang, offset, or cavity. This additional material prevents the

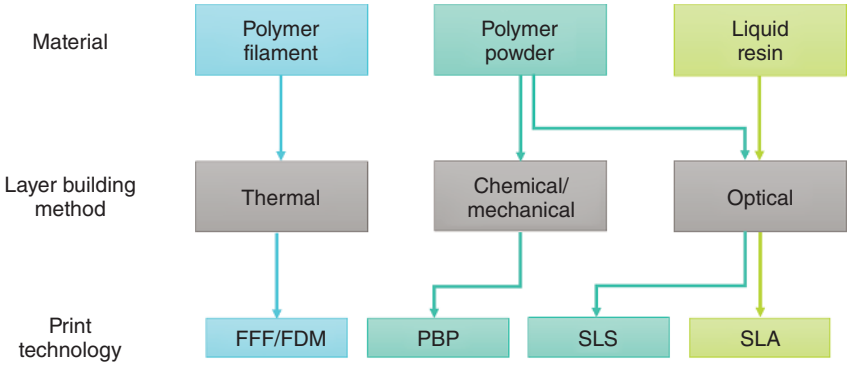

Figure 1.3 Overview of material types used with specific layer building methods in 3D/4D printing.

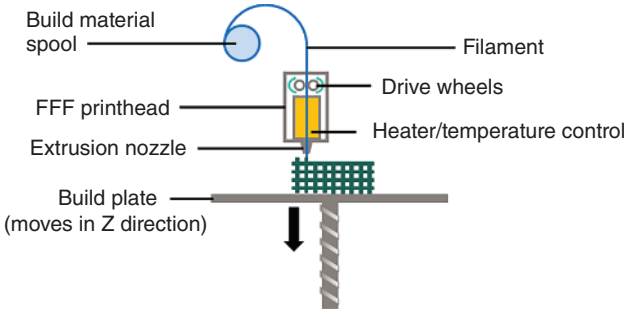

Figure 1.4 Schematic of FFF process.

component part from collapsing during the building process. The support material itself can be easily removed after the building process by breaking it off or dissolving it in a warm water bath.

The FFF approach allows fabrication of structures with controllable pore size and porosity by changing the material deposition amount, the spacing between the material paths, and the height interval (z axis). The most important material selection criteria for FFF materials are heat transfer characteristics and rheology because the FFF approach requires processable prepolymers as the building materials (filaments).

A major benefit of FFF printing is that the polymer filaments can be manufactured with hot melt extrusion (HME). This means that the knowledge and acceptance of HME-manufactured materials is already assured. However, the FFF process usually requires tight specifications for the filaments. Melocchi et al. [25] pointed out the need for homogeneous filaments with a minimum length of 25 cm, circular cross section, and consistent diameter as well as diameter tolerances (1.75 ± 0.05 mm) for filaments made of hydroxypropylcellulose (Klucel™ LF, Ashland). Undersized filament diameter led to the formation of air bubbles within the printed material and an oversized one resulted in clogging of the tip [25]. The diameter of the extruded filaments depends not only on the diameter of the extrusion die but also on the relaxation of the polymer and the speed of the conveying belt (Figure 1.5). Although both diameter and variance along the length of the filament matter, consistency is more important than exactly reaching 1.75 mm in diameter.

Suitable polymeric materials for FFF printer are thermoplastic and become molten at reasonably low heating temperatures (usually lower than 250 °C). They solidify fast enough (sufficiently high glass transition temperature) so that they hold their shape when hardened. Furthermore, the materials possess specific mechanical properties.

To predict the mechanical behavior of these materials, it is critical to understand the material properties of the raw material as well as the effect that the process parameters of FFF have on those mechanical properties [26]. There are various options for processing parameters such as layer thickness, build orientation, raster angle, raster width, and raster-to-raster air gap, all of which can significantly affect the mechanical properties and performance of the

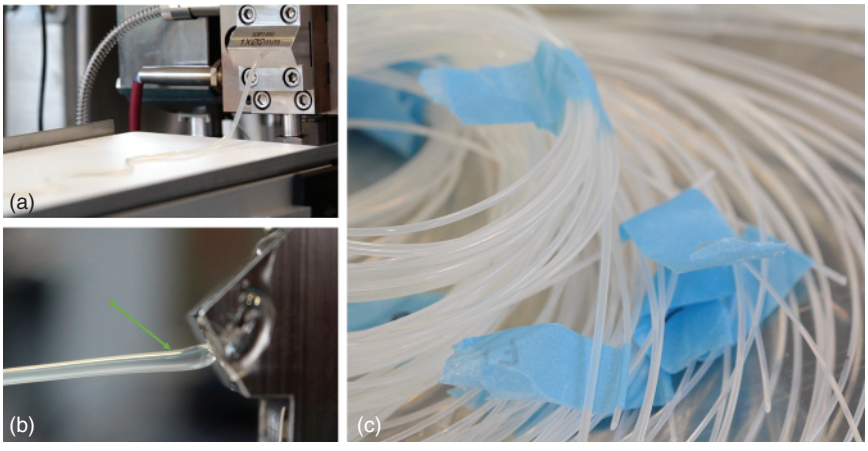

Figure 1.5 (a) Hot melt extrusion of hydroxypropylcellulose (HPC) filaments suitable for FFF. (b) Polymer relaxation (die swell) of HPC after leaving the extrusion die. (c) HPC filaments varying in diameter (<1.8 mm).

Table 1.2 Variables that can affect mechanical properties of printed materials.

Process variables	Design variables	Material variables
Build orientation	Printer model	Rheological properties
Layer thickness	Process type	Density of the unprocessed material
Raster angle	Extrusion nozzle diameter	Thermal properties of polymer and other ingredients
Raster width	Software	Formulation; miscibility and concentration of the components
Raster-to-raster air gap		Filament diameter
Fill pattern		Uniformity of filament diameter
Material deposition speed/amount		
Extrusion temperature		
Chamber temperature		
Environmental conditions (e.g. humidity)		

FFF material [27]. An overview of variables that might affect the mechanical properties of printed materials is given in Table 1.2.

Originally, acrylonitrile butadiene styrene (ABS) served as the feedstock material, delivered as fibers from spools. However, the range of materials that can be processed effectively is increasing, including new materials and polymer blends in the filament form. Other material options include polycarbonate (PC), polypropylene (PP), polyphenylsulfone (PPSF), polyglycolic acid

(PGA), poly(L-glutamic acid) (PLGA) and PCL, polydioxanone (PDO), and poly(ether-ether-ketone) (PEEK).

For biomedical purposes, biodegradable materials have been frequently used to replace metallic implants for internal fixation. For instance, PGA- or PLA-based screws and pins have been widely used for orthopedic surgery, offering the advantage of being resorbable [28]. With the use and development of 3D printing technologies such as FFF rising, more complex shapes are possible to print.

PLGA has been previously used with FFF to create scaffolds [29–31]; however, the comparably high glass transition temperature of 40–60 °C presents challenges to the extrusion process because a higher extrusion temperature is required to create the right material flow properties for extrusion from the nozzle and for fusion of the layers [30, 31].

Another polymer that has been widely used to fabricate bioresorbable scaffolds for bone tissue engineering applications is PCL. In contrast to PLGA, it has a low melting temperature of approximately 60 °C, low glass transition temperature of −60 °C, and high thermal stability [23, 32], although still being biodegradable by hydrolysis [33, 34]. Apart from bone tissue engineering, PCL can also be used for the preparation of implantable devices, such as drug-loaded implants [35], or long-lasting implantable intrauterine systems for birth control [36].

Other melt-extrudable polymer-based medical devices have incorporated PEEK because of its cell biocompatibility and desirable mechanical properties such as the elastic modulus being comparable to that of cortical bone, which results in reduced stress shielding after implantation [37]. Although more often processed using selective laser sintering (SLS)[38], it can also be formed with FFF, although it is quite challenging to process because of its very high melting temperature[39, 40].

Overall, the main advantages of the FFF process are that it does not require toxic or organic solvents, and the use of filaments allow for continuous low-cost production, with high flexibility in handling and processing of materials. Despite these advantages, the FFF process includes restrictions with regard to the material properties of the feedstock filament material necessary to feed it through the rollers and nozzle. Any changes in the properties of the material require considerable effort to recalibrate the feeding parameters. Additionally, parts manufactured by the FFF technique show some dimensional inaccuracy compared to other additive manufacturing techniques such as SLS because of the variety of conflicting and interacting process parameters that affect dimensional accuracy [41].

1.5.2 Powder Bed Printing (PBP) – Droplet-Based Systems

Powder bed printing (PBP) was developed at the Massachusetts Institute of Technology [42] and utilizes a liquid binder, delivered by an inkjet printhead, to build objects layer-by-layer from a bed of powder. The process begins by evenly spreading a layer of powder onto the build plate. The layer typically has a thickness of 200 μm and consists of powder with a particle size range of 50–100 μm [43]. The inkjet printhead then deposits droplets of the liquid binder solution onto the powder surface. The powder is solidified by the binder solution in the shape of the

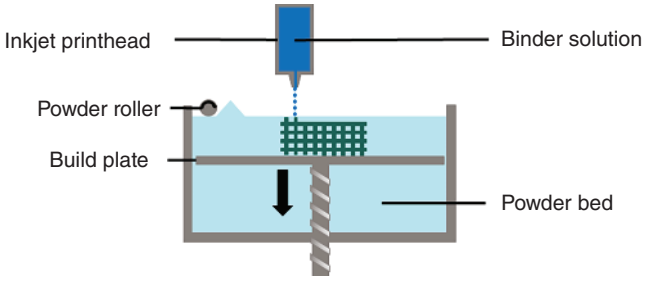

Figure 1.6 Schematic illustration of 3D printing by PBP.

two-dimensional cross section of that layer. The build plate is then lowered to the depth of the next layer and a new even layer of powder is spread across the surface in readiness for the printing of the new cross section. The process continues until the complete object is constructed within the powder bed. Overhanging structures and pores within the object are supported by the unbound powder during the printing process. Once complete, the object is removed from the surrounding unbound powder, including the removal of unbound powder from cavities and pores within the finished structure. The ease with which the object can be depowdered depends on the complexity of the design and may sometimes require the use of an air gun. The liquid binding of the powder tends to result in porous structures, which are sometimes sintered in order to improve the surface finish and mechanical strength [44, 45]. The process is illustrated in Figure 1.6.

The concepts behind inkjet printing were first described by Lord Rayleigh in the late nineteenth century [46, 47]. Development of these concepts has resulted in devices that can deliver either a continuous stream of droplets, known as continuous ink jetting (CIJ), or a drop-on-demand (DOD) ejection of droplets. The CIJ process releases a continuous stream of charged droplets, which are directed by electrostatic plates into the powder bed, or deviated into a waste recirculation line. On the other hand, the DOD process only dispenses the binder liquid droplets when required by the printing process, thus making it less wasteful than the CIJ process. Additionally, DOD is more precise than CIJ, with the ability to control droplet volume within a range of 1–300 pl [48, 49] at delivery frequencies of up to 10 000 Hz [50]. Production of droplets within a DOD printhead can be achieved by thermal or piezoelectrc methods. Thermal printheads consist of a thin film resistor that heats up rapidly when an electric pulse is applied. A superheated vapor bubble is formed, which expands and ejects a droplet from the print nozzle. Subsequent collapse of the bubble creates a partial vacuum, into which fresh binder solution is pulled [51]. Temperatures as high as 300 °C can be reached at the resistor surface, but the exposure time is in the order of milliseconds, and only a small fraction of the liquid, approximately 0.5% by volume, is heated, thus minimizing the potential effect of degradation of any thermally labile components [52]. Droplet formation within a piezoelectric printhead is a result of pressure waves that are induced within the liquid when a voltage is applied to the surrounding piezoelectric transducer causing it to deform. The liquid reservoir then refills once the piezoelectric material regains its original shape. In contrast

to thermal inkjet printheads, the piezoelectric process is thermally constant and can be carried out at room temperature or in a localized cold environment [53].

A wide variety of powders, commonly utilized in medical applications, have been used in PBP in combination with suitable binders. It has been said that any combination of a powdered material with a binder that has low enough viscosity to form droplets could be used [54]. The physical and chemical properties of the binder solution need to be controlled in the PBP process. For successful delivery from the printheads, the viscosity of the binder solution needs to be in the range of 5–20 Pa s and the surface tension in the range of 35–40 mJ N^{-1} [51]. If an organic solvent is used in the binder solution, care must be taken to ensure the printhead is compatible with the solvent, as some organic solvents can dissolve the polymers used in most printheads [55]. The powder must have sufficient flow to enable it to be spread evenly to the thickness required for each layer. It must also be able to be removed easily from within the cavities and pores of the finished object. A number of synthetic polymers, including PCL, poly(lactide-*co*-glycolide), and PLA, have been used with organic solvent-based binders [56–58]. Natural polymers such as starch, dextran, and gelatin have been used in combination with water as a binder [44, 59]. Calcium phosphate-based bioceramics have also been used in PBP biomedical applications with acid- and solvent-based binder solutions [60]. There is also the ability to incorporate additional components within the powder bed or binder solution to expand the versatility of the PBP process. The additional components could be active pharmaceutical ingredients for drug delivery [61, 62] or biological agents such as peptides, proteins, polysaccharides, DNA plasmids, or cells [55].

1.5.3 Stereolithographic (SLA) Printing – Resin-Based Systems

SLA is a well-established 3D printing technology. In simple terms, it uses UV or visible light to solidify liquid, photocurable polymer resins. Objects are built up through sequential illumination of thin layers of resin, either by tracing a pattern with a laser beam or projecting the pattern with a digital projector, which solidifies the illuminated resin. Construction of a 3D object can be achieved in two ways. The object can be built from the bottom-up by illumination of the layer pattern on the upper surface of a bath of resin. Once the layer is complete, the build platform is lowered by the depth of the next layer and a blade is swept across the surface to apply a smooth layer of fresh resin. The new layer of resin is then illuminated with the next layer pattern. The alternative approach is to build the object from the top-down. In this case, the resin is placed in a bath with a base made of a UV–vis transparent material, such as polyethylene terephthalate (PET) [63]. The layer pattern is illuminated through the base window, onto the lower surface of the resin. The solidified layer is then raised upward by one layer thickness, liquid resin fills the space below the solid layer, and is illuminated with the next layer pattern. Schematic representations of these two approaches are illustrated in Figure 1.7.

In both cases, the depth of curing of each layer is slightly larger than the step movement of the build platform in the *z*-direction. Unreacted functional groups in the solid layer can then polymerize with the exposed resin in the new layer,

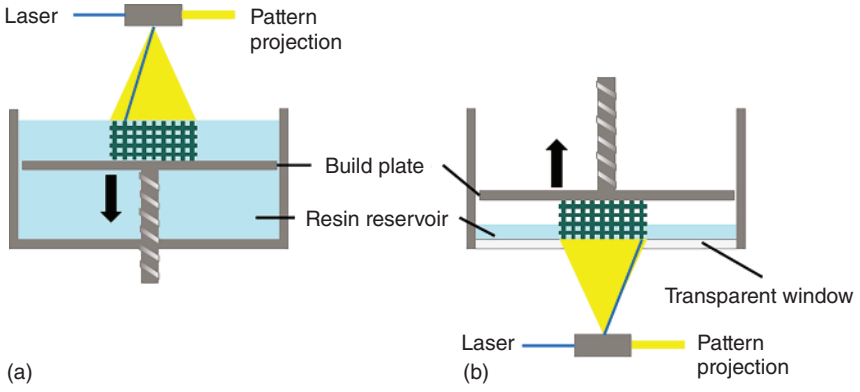

Figure 1.7 Schematic illustration of SLA process: (a) bottom-up process and (b) top-down process.

thus ensuring good adherence between each layer of the build. At the end of the process, when all layers have been completed, excess resin is drained and washed off. The completed object is often exposed to a final curing step using UV light to ensure full conversion of unreacted functional groups in the polymer.

The top-down process offers some advantages over the bottom-up process, but there are also some disadvantages. The consumption of resin is significantly lower in the top-down process because of not having to immerse the entire object in the resin. The time taken for the resin surface to settle and be swept by a blade is not required in the top-down process. Additionally, the top-down process exhibits greater control of layer thickness. This is a result of forming completely flat layers at the bottom of the resin tank. There is also no exposure to the air, which occurs in the bottom-up process, and can lead to oxygen inhibition of the polymerization reaction. However, because of the photopolymerization of each layer occurring in contact with the transparent window, there is the possibility of adherence between the solidifying layer and the window. Consequently, as the build platform rises upward, it could result in damage to the newly formed layer. Another potential drawback occurs during the manufacture of larger, heavier objects, where separation between the build platform and the object may occur, or weak sections may break. Addition of supports for weak sections can alleviate this problem.

The layer pattern can be transmitted to the surface of the resin by tracing the pattern with a single laser beam, known as scanning lithography or direct writing. Alternatively, it can be achieved by projecting the entire pattern onto the surface of the resin using a digital mask generator such as a digital micromirror device (DMD), known as projection-based SLA or the dynamic mask method. Projection-based SLA processes are less expensive than the direct writing process because of not requiring an expensive laser system. Projection of the entire layer pattern onto the resin surface enables a complete layer of resin to be cured simultaneously. The resultant build time is significantly reduced compared to direct writing, as it is dependent only on layer thickness and required exposure time, rather than also size in the *xy*-plane and the number of structures being built [64].

A combination of the scanning and projection methods has been developed by Emami and coworkers [63, 65] described as scanning–projection-based SLA. The projected image is continually updated as it is scanned over the surface of the layer being built. This allows larger objects to be constructed at higher resolution.

The resolution of the object being built is governed by a combination of the diameter of the laser beam or pixel size of the projection device and the curing depth of each layer. The depth of cure for each resin is determined by the amount of energy applied. This can be controlled by adjusting the power of the light source and the length of time the light is applied onto the resin. The complex kinetics of the photopolymerization curing process has been described in detail [66]. However, a simpler, semiempirical model based on the Beer–Lambert law has been described [67]. Equation (1.1) relates the cure depth in microns (C_d) to the dose of light irradiation, E (mJ cm^{-2}).

$$C_d = D_p \ln\left(\frac{E}{E_c}\right) \tag{1.1}$$

Determining the cure depth, or layer thickness, and plotting it against the applied radiation produce what has been called a working curve, which can then be used to determine the correct settings for the SLA process. SLA resins are characterized by a critical energy, E_c, and a penetration depth, D_p. Penetration depth, D_p, is directly related to the extinction coefficient in the Beer–Lambert equation. When the applied dose of irradiation, E, is greater than the critical energy, E_c, the resin solidifies from the surface. The concentrations of photoinitiator, dissolved oxygen, and other inhibiting species will all affect the value of E_c.

To ensure the effective layer-to-layer bonding, the value of C_d should be slightly higher than the layer thickness. This, however, results in additional curing in the preceding layer, potentially resulting in polymerization of voids within the design of the object being fabricated. For porous structures, such as scaffolds for tissue engineering, the effect of polymerization in the voids could be significant. Accurate control of the polymerization process can minimize the effect of filling voids with solidified resin. This can be achieved by reducing the light penetration depth, D_p, through the use of higher concentrations of photoinitiator, or the inclusion of nonreactive components such as dyes or UV absorbers [68]. The negative impact of reducing the value of D_p is that the build time is increased.

Possible limitations of SLA for biomedical applications include the small number of biocompatible resins that are suitable for the process and the complexities associated with using more than a single resin in the construction of the finished object. The number of suitable, photocurable resins is increasing and examples include poly(propylene fumarate) [69], poly(ε-caprolactone-*co*-trimethylene carbonate) [70], poly(D,L-lactide) [71], PCL [72], and PEG [73–76]. Resins with reported 4D properties based on soybean-oil-epoxized acrylate have also been reported by Miao et al. [14]. Overcoming the limitation of incorporating more than one resin into an object is more difficult. Techniques have been developed in which sequential polymerization and rinsing steps allow multiple resins to be built into each layer [73, 77]. A simple, automated method to switch between different resins would greatly expand the potential of the SLA technique.

1.5.4 Selective Laser Sintering (SLS) Printing – Laser-Based Systems

SLS was introduced soon after the SLA technique, but it primarily employs semicrystalline, particulate thermoplastic prepolymer as the building material. The technique involves a bed of tightly compacted powdered particles that is preheated close to the melting transition temperature. A laser beam is traced over the surface of the powder bed to bind the powder particles together. During the printing process, the laser draws a specific pattern onto the surface of the powder bed. After finishing the sintering of the first layer, the building platform is lowered by 100–200 µm and fresh powder is spread by a roller to build a new layer on top of the previous one. The resulting 3D printed object is built layer-by-layer and is finally recovered from underneath the powder bed. An illustration of the SLS process is shown in Figure 1.8.

Localized thermal sintering of particles is achieved by additional energy input from a high-power carbon dioxide (CO_2) laser, which scans the surface of the powder bed in a specific pattern and selectively melts the powder. The entire fabrication chamber is sealed and maintained at a temperature just below the melting point of the plastic powder. Thus, heat from the laser needs only to elevate the temperature slightly to cause sintering, greatly speeding up the process.

Especially for the selection of (new) laser sinter materials, an understanding of the different SLS subprocesses is essential. Different material properties and process parameters may affect the structural and mechanical properties of printed objects [78], and it is important to find a balance between effective sintering and avoiding polymer degradation that comes with overheating due to laser power and energy density [79]. SLS process parameters include part bed temperature, feed bed temperature, powder layer thickness, laser power, scan spacing, number of scans, time between layers, roller speed, build size, and heating/cooling rates, and these parameters are set differently according to powder properties and requirements of the application to achieve an optimum quality [80].

The basic material developed for SLS technology is a freely poured (loose) or slightly compacted polymeric powder, typically with a particle size in the range

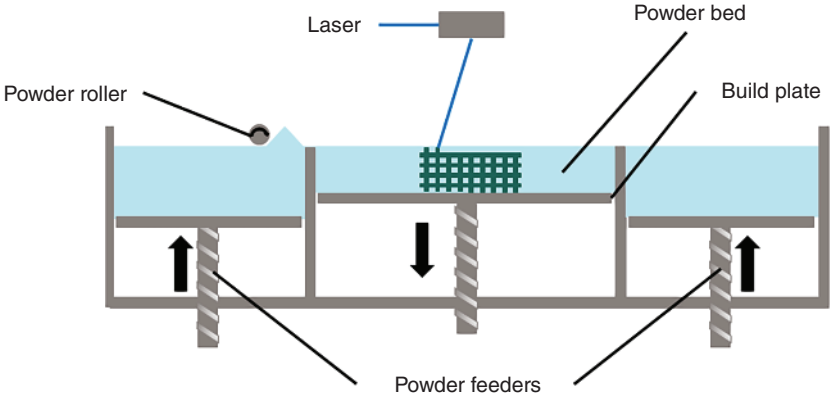

Figure 1.8 Schematic of SLS process using a CO_2 laser to locally fuse powder particles on the surface of a preheated build chamber that is incrementally lowered as the process progresses.

of several microns to several hundred microns [81]. The application of powders aims to apply a smooth, dense, and uniform powder layer when displaced by a roller or other spreading mechanism. After each finished layer, the new powder layer needs to be heated as fast as possible over its crystallization temperature to reach a fully melted state necessary for complete bonding between powder particles and to avoid cooling of the already finished layer, which can potentially cause shrinking and deformation of the sintered layer. Critical material attributes for deposition and laser sintering of the powder include powder density, particle shape, particle size distribution, and flowability [82, 83].

The most commonly used materials are powdered forms of plastics, ceramics, and metal alloys that require high temperatures and high-energy lasers to be sintered. These harsh printing conditions are the reason that the use of SLS printing in the medical field has been limited to medical instruments and implants, for example [38], or drug delivery devices where the drug was included after the printing process to circumvent the problem that the energy input of the high-power laser may degrade components if they are used as the starting material [84]. SLS polymer feedstock materials tend to be thermoplastic polymers that are either (semi)-crystalline polymers such as polyamide (PA, nylon) [85], poly(ABS), PEEK [38], and polyether block amide (PEBA) [86] or amorphous materials such as PC, and more recently polystyrene (PS), showing a different thermal behavior. The selection criteria of the semicrystalline polymers primarily include a broad process temperature window between the melting (T_m) and recrystallization temperature, a narrow melt transition, and a high melting enthalpy to minimize unwanted sintering [82], whereas the selection criteria for amorphous materials are somewhat different. Amorphous polymers tend to yield weaker, more porous structures than the semicrystalline polymer powders [87], and they do not undergo the significant dimensional contraction associated with crystallization as the process temperature is reduced [88]. Overall, glass transition temperature (T_g) and melting temperature (T_m) play important roles in the selection of process parameters and directly affect the mechanical properties of the SLS components. Other thermal properties such as specific heat capacity and thermal conductivity of polymers have great influence on the fabrication process as well [80].

Using SLS technology allows for complex 3D structures to be printed without the use of (organic) solvents. Moreover, as long as the material is in powdered form and can fuse but will not decompose under the laser beam, it can be used with SLS [89]. This opened the way for many biomedical applications ranging from the use of PEEK to produce non-resorbable implants for tissue engineering [38] and the production of bioactive implants and tissue scaffolds using composites of high-density polyethylene (HDPE) reinforced with hydroxyapatite (HA)[90], to biodegradable substitutes for tissue engineering to repair or replace damaged tissues such as PCL-[89]and poly-(L-lactic) acid (PLLA)[91]-fabricated scaffolds.

The potential disadvantages of SLS technology are the poor surface and dimensional accuracy and materials that sometimes require post-processing treatments that are considered critical for complex and controlled 3D printed structures.

1.6 Conclusions and Perspectives

Although the field of 4D printing in biomedical applications is just starting to emerge, the available pioneering examples demonstrate the possibility to incorporate the time scale into 3D printing to achieve transformation of printed objects along prescribed paths. It is necessary to develop new stimuli-responsive smart materials that, in addition to excellent biocompatibility, also possess appropriate rheological properties to ensure printability, appropriate mechanical properties, and stabilization mechanisms for the desired application and offer an effective interplay between cellular viability, function, and dynamic modulation of the printed objects. Merging these smart biomaterials within innovative technologies, 4D bioprinting is expected to become the next big thing to create transformable objects in biomedical applications, eventually mimicking the complex, dynamic deformation of native tissues such as the pumping behavior of the heart and the peristaltic movements of the gastrointestinal tract, among others.

References

1 Barnatt, C. (2013). *3D Printing: The Next Industrial Revolution*. CreateSpace Independent Publishing Platform.

2 Ionita, C.N., Mokin, M., Varble, N. et al. (eds.) (2014). Challenges and limitations of patient-specific vascular phantom fabrication using 3D Polyjet printing. In: *SPIE Medical Imaging*. SPIE.

3 Ozbolat, I.T. (2015). Bioprinting scale-up tissue and organ constructs for transplantation. *Trends in Biotechnology* 33 (7): 395–400.

4 Choong, C., Maleksaeedi, S., Eng, H. et al. (2017). 4D printing of high performance shape memory polymer using stereolithography. *Materials & Design* 126: 219–225.

5 Raman, R., Cvetkovic, C., Uzel, S.G.M. et al. (2016). Optogenetic skeletal muscle-powered adaptive biological machines. *Proceedings of the National Academy of Sciences* 113 (13): 3497–3502.

6 Morgan, N.B. (2004). Medical shape memory alloy applications – the market and its products. *Materials Science and Engineering: A* 378 (1): 16–23.

7 Tibbits, S. (2013). The emergence of "4D printing". https://www.ted.com/talks/skylar_tibbits_the_emergence_of_4d_printing/transcript?language=en (accessed 12 January 2018).

8 Gladman, A.S., Matsumoto, E.A., Nuzzo, R.G. et al. (2016). Biomimetic 4D printing. *Nature Materials* 15 (4): 413–418.

9 Campbell, T.A., Tibbits, S., and Garrett, B. (2014). The Next Wave: 4D Printing Programming the Material World. Technical report. Atlantic Council, USA.

10 Breger, J.C., Yoon, C., Xiao, R. et al. (2015). Self-folding thermo-magnetically responsive soft microgrippers. *ACS Applied Materials & Interfaces* 7 (5): 3398–3405.

11 Zarek, M., Mansour, N., Shapira, S., and Cohn, D. (2017). 4D printing of shape memory-based personalized endoluminal medical devices. *Macromolecular Rapid Communications* 38 (2): 1600628.

12 Huang, W.M., Song, C.L., Fu, Y.Q. et al. (2013). Shaping tissue with shape memory materials. *Advanced Drug Delivery Reviews* 65 (4): 515–535.

13 Li, G., Zhang, H., Fortin, D. et al. (2015). Poly(vinyl alcohol)–poly(ethylene glycol) double-network hydrogel: a general approach to shape memory and self-healing functionalities. *Langmuir* 31 (42): 11709–11716.

14 Miao, S., Zhu, W., Castro, N.J. et al. (2016). 4D printing smart biomedical scaffolds with novel soybean oil epoxidized acrylate. *Science Reports* 627226.

15 Hao, L., Gwangjun, G., Seong Yong, K. et al. (2016). Magnetic actuated pH-responsive hydrogel-based soft micro-robot for targeted drug delivery. *Smart Materials and Structures* 25 (2): 027001.

16 Zhao, X., Kim, J., Cezar, C.A. et al. (2011). Active scaffolds for on-demand drug and cell delivery. *Proceedings of the National Academy of Sciences* 108 (1): 67–72.

17 Unger, K., Salzmann, P., Masciullo, C. et al. (2017). Novel light-responsive biocompatible hydrogels produced by initiated chemical vapor deposition. *ACS Applied Materials & Interfaces* 9 (20): 17408–17416.

18 Zhang, L., Liang, H., Jacob, J., and Naumov, P. (2015). Photogated humidity-driven motility. *Nature Communications* 6: 7429.

19 Zhang, K., Geissler, A., Standhardt, M. et al. (2015). Moisture-responsive films of cellulose stearoyl esters showing reversible shape transitions. *Scientific Reports* 511011.

20 Jamal, M., Kadam, S.S., Xiao, R. et al. (2013). Bio-origami hydrogel scaffolds composed of photocrosslinked PEG bilayers. *Advanced Healthcare Materials* 2 (8): 1142–1150.

21 Raviv, D., Zhao, W., McKnelly, C. et al. (2014). Active printed materials for complex self-evolving deformations. *Scientific Reports* 4: 7422.

22 Kim, G.D. and Oh, Y.T. (2008). A benchmark study on rapid prototyping processes and machines: quantitative comparisons of mechanical properties, accuracy, roughness, speed, and material cost. *Proceedings of the Institution of Mechanical Engineers, Part B: Journal of Engineering Manufacture* 222 (2): 201–215.

23 Gibson, I., Rosen, D., and Stucker, B. (2015). *Additive Manufacturing Technologies – 3D Printing, Rapid Prototyping, and Direct Digital Manufacturing*. New York: Springer-Verlag.

24 Sun, Q., Rizvi, G.M., Bellehumeur, C.T., and Gu, P. (2008). Effect of processing conditions on the bonding quality of FDM polymer filaments. *Rapid Prototyping Journal* 14 (2): 72–80.

25 Melocchi, A., Parietti, F., Loreti, G. et al. (2015). 3D printing by fused deposition modeling (FDM) of a swellable/erodible capsular device for oral pulsatile release of drugs. *Journal of Drug Delivery Science and Technology* 30: 360–367.

26 Novakova-Marcincinova, L. and Novak-Marcincin, J. (2012). Testing of materials for rapid prototyping fused deposition modelling technology.

International Journal of Mechanical, Aerospace, Industrial, Mechatronic and Manufacturing Engineering 6 (10): 2082–2085.

27 Sood, A.K., Ohdar, R.K., and Mahapatra, S.S. (2010). Parametric appraisal of mechanical property of fused deposition modelling processed parts. *Materials & Design* 31 (1): 287–295.

28 Agrawal, C.M., Niederauer, G.G., and Athanasiou, K.A. (1995). Fabrication and characterization of PLA–PGA orthopedic implants. *Tissue Engineering* 1 (3): 241–252.

29 Kim, J.Y. and Cho, D.-W. (2009). Blended PCL/PLGA scaffold fabrication using multi-head deposition system. *Microelectronic Engineering* 86 (4): 1447–1450.

30 Park, S.H., Park, D.S., Shin, J.W. et al. (2012). Scaffolds for bone tissue engineering fabricated from two different materials by the rapid prototyping technique: PCL versus PLGA. *Journal of Materials Science: Materials in Medicine* 23 (11): 2671–2678.

31 Kim, J., McBride, S., Tellis, B. et al. (2012). Rapid-prototyped PLGA/β-TCP/hydroxyapatite nanocomposite scaffolds in a rabbit femoral defect model. *Biofabrication* 4 (2): 025003.

32 Hutmacher, D.W., Schantz, T., Zein, I. et al. (2001). Mechanical properties and cell cultural response of polycaprolactone scaffolds designed and fabricated via fused deposition modeling. *Journal of Biomedical Materials Research* 55 (2): 203–216.

33 Piskin, E., Nimet, B., Egri, S., and Isoglu, I.A. (2007). Electrospun matrices made of poly(α-hydroxy acids) for medical use. *Nanomedicine* 2 (4): 441–457.

34 Pitt, C.G., Chasalow, F.I., Hibionada, Y.M. et al. (1981). Aliphatic polyesters. I. The degradation of poly(ε-caprolactone) in vivo. *Journal of Applied Polymer Science* 26 (11): 3779–3787.

35 Kempin, W., Franz, C., Koster, L.-C. et al. (2017). Assessment of different polymers and drug loads for fused deposition modeling of drug loaded implants. *European Journal of Pharmaceutics and Biopharmaceutics* 115: 84–93.

36 Holländer, J., Genina, N., Jukarainen, H. et al. (2016). Three-dimensional printed PCL-based implantable prototypes of medical devices for controlled drug delivery. *Journal of Pharmaceutical Sciences* 105 (9): 2665–2676.

37 Sobieraj, M.C. and Rimnac, C.M. (2012). Chapter 5 – Fracture, fatigue, and notch behavior of PEEK A2. In: *PEEK Biomaterials Handbook* (ed. S.M. Kurtz), 61–73. Oxford: William Andrew Publishing.

38 Schmidt, M., Pohle, D., and Rechtenwald, T. (2007). Selective Laser Sintering of PEEK. *CIRP Annals – Manufacturing Technology* 56 (1): 205–208.

39 Vaezi, M. and Yang, S. (2015). Extrusion-based additive manufacturing of PEEK for biomedical applications. *Virtual and Physical Prototyping* 10 (3): 123–135.

40 Valentan, B., Kadivnik, Ž., Brajlih, T. et al. (2013). Processing poly(ether etherketone) an a 3D printer for thermoplastic modelling. *Materiali in Tehnologije* 47 (6): 715–721.

41 Mohamed, O.A., Masood, S.H., and Bhowmik, J.L. (2015). Optimization of fused deposition modeling process parameters: a review of current research and future prospects. *Advances in Manufacturing* 3 (1): 42–53.

42 Sachs, E.M., Haggerty, J.S., Cima, M.J., and Williams, P.A. (1993). Three-dimensional printing techniques. US Patent 5, 204,055, 20 April 1993.

43 Pfister, A., Landers, R., Laib, A. et al. (2004). Biofunctional rapid prototyping for tissue-engineering applications: 3D bioplotting versus 3D printing. *Journal of Polymer Science Part A: Polymer Chemistry* 42 (3): 624–638.

44 Seitz, H., Rieder, W., Irsen, S. et al. (2005). Three-dimensional printing of porous ceramic scaffolds for bone tissue engineering. *Journal of Biomedicals Materials Research Part B Applied Biomaterials* 74 (2): 782–788.

45 Lee, J.W., Kim, J.Y., and Cho, D.W. (2010). Solid free-form fabrication technology and its application to bone tissue engineering. *International Journal of Stem Cells* 3 (2): 85–95.

46 Rayleigh, L. (1878). The influence of electricity on colliding water drops. *Proceedings of the Royal Society of London* 28: 406–409.

47 Rayleigh, L. (1879). On the capillary phenomena of jets. *Proceedings of the Royal Society of London* 29: 71–97.

48 Sekitani, T., Noguchi, Y., Zschieschang, U. et al. (2008). Organic transistors manufactured using inkjet technology with subfemtoliter accuracy. *Proceedings of the National Academy of Sciences of the United States of America* 105 (13): 4976–4980.

49 Singh, M., Haverinen, H.M., Dhagat, P., and Jabbour, G.E. (2010). Inkjet printing – process and its applications. *Advanced Materials* 22 (6): 673–685.

50 Demirci, U. and Montesano, G. (2007). Single cell epitaxy by acoustic picolitre droplets. *Lab on a Chip* 7 (9): 1139–1145.

51 Shirazi, S.F.S., Gharehkhani, S., Mehrali, M. et al. (2015). A review on powder-based additive manufacturing for tissue engineering: selective laser sintering and inkjet 3D printing. *Science and Technology of Advanced Materials* 16 (3): 033502.

52 Alomari, M., Mohamed, F.H., Basit, A.W., and Gaisford, S. (2015). Personalised dosing: printing a dose of one's own medicine. *International Journal of Pharmaceutics* 494 (2): 568–577.

53 Sumerel, J., Lewis, J., Doraiswamy, A. et al. (2006). Piezoelectric ink jet processing of materials for medical and biological applications. *Biotechnology Journal* 1 (9): 976–987.

54 Guo, N. and Leu, M.C. (2013). Additive manufacturing: technology, applications and research needs. *Frontiers of Mechanical Engineering* 8 (3): 215–243.

55 Chia, H.N. and Wu, B.M. (2015). Recent advances in 3D printing of biomaterials. *Journal of Biological Engineering* 9 (1): 4.

56 Wu, B.M., Borland, S.W., Giordano, R.A. et al. (1996). Solid free-form fabrication of drug delivery devices. *Journal of Controlled Release* 40 (1): 77–87.

57 Kim, S.S., Utsunomiya, H., Koski, J.A. et al. (1998). Survival and function of hepatocytes on a novel three-dimensional synthetic biodegradable polymer scaffold with an intrinsic network of channels. *Annals of Surgery* 228 (1): 8–13.

58 Zeltinger, J., Sherwood, J.K., Graham, D.A. et al. (2001). Effect of pore size and void fraction on cellular adhesion, proliferation, and matrix deposition. *Tissue Engineering* 7 (5): 557–572.

59 Lam, C.X.F., Mo, X.M., Teoh, S.-H., and Hutmacher, D. (2002). Scaffold development using 3D printing with a starch-based polymer. *Materials Science and Engineering C: Materials for Biological Applications* 20 (1/2): 49–56.

60 Brunello, G., Sivolella, S., Meneghello, R. et al. (2016). Powder-based 3D printing for bone tissue engineering. *Biotechnology Advances* 34 (5): 740–753.

61 Acosta-Vélez, G. and Wu, B.M. (2016). 3D pharming: direct printing of personalized pharmaceutical tablets. *Polymer Sciences* 2 (1:3).

62 Alhnan, M.A., Okwuosa, T.C., Sadia, M. et al. (2016). Emergence of 3D printed dosage forms: opportunities and challenges. *Pharmaceutical Research* 33 (8): 1817–1832.

63 Emami, M.M., Barazandeh, F., and Yaghmaie, F. (2014). Scanning-projection based stereolithography: method and structure. *Sensors and Actuators A: Physical* 218 (Supplement C): 116–124.

64 Melchels, F.P.W., Feijen, J., and Grijpma, D.W. (2010). A review on stereolithography and its applications in biomedical engineering. *Biomaterials* 31 (24): 6121–6130.

65 Emami, M.M., Barazandeh, F., and Yaghmaie, F. (2015). An analytical model for scanning-projection based stereolithography. *Journal of Materials Processing Technology* 219 (Supplement C): 17–27.

66 Andrzejewska, E. (2001). Photopolymerization kinetics of multifunctional monomers. *Progress in Polymer Science* 26 (4): 605–665.

67 Jacobs, P.F. (1993). *Rapid Prototyping and Manufacturing: Fundamentals of StereoLithography*. Dearborn, MI: Society of Manufacturing Engineers.

68 Heller, C., Schwentenwein, M., Russmueller, G. et al. (2009). Vinyl esters: low cytotoxicity monomers for the fabrication of biocompatible 3D scaffolds by lithography based additive manufacturing. *Journal of Polymer Science Part A: Polymer Chemistry* 47 (24): 6941–6954.

69 Cooke, M.N., Fisher, J.P., Dean, D. et al. (2003). Use of stereolithography to manufacture critical-sized 3D biodegradable scaffolds for bone ingrowth. *Journal of Biomedial Materials Research Part B Applied Biomaterials* 64 (2): 65–69.

70 Matsuda, T. and Mizutani, M. (2002). Liquid acrylate-endcapped biodegradable poly(epsilon-caprolactone-co-trimethylene carbonate). II. Computer-aided stereolithographicmicroarchitectural surface photoconstructs. *Journal of Biomedial Materials Research* 62 (3): 395–403.

71 Melchels, F.P., Feijen, J., and Grijpma, D.W. (2009). A poly(DL-lactide) resin for the preparation of tissue engineering scaffolds by stereolithography. *Biomaterials* 30 (23–24): 3801–3809.

72 Elomaa, L., Teixeira, S., Hakala, R. et al. (2011). Preparation of poly(epsilon-caprolactone)-based tissue engineering scaffolds by stereolithography. *Acta Biomaterialia* 7 (11): 3850–3856.

73 Arcaute, K., Mann, B.K., and Wicker, R.B. (2006). Stereolithography of three-dimensional bioactive poly(ethylene glycol) constructs with encapsulated cells. *Annals of Biomedical Engineering* 34 (9): 1429–1441.

74 Dhariwala, B., Hunt, E., and Boland, T. (2004). Rapid prototyping of tissue-engineering constructs, using photopolymerizable hydrogels and stereolithography. *Tissue Engineering* 10 (9–10): 1316–1322.

75 Lu, Y., Mapili, G., Suhali, G. et al. (2006). A digital micro-mirror device-based system for the microfabrication of complex, spatially patterned tissue engineering scaffolds. *Journal of Biomedial Materials Research Part A* 77 (2): 396–405.

76 Arcaute, K., Mann, B., and Wicker, R. (2010). Stereolithography of spatially controlled multi-material bioactive poly(ethylene glycol) scaffolds. *Acta Biomaterialia* 6 (3): 1047–1054.

77 Mapili, G., Lu, Y., Chen, S., and Roy, K. (2005). Laser-layered microfabrication of spatially patterned functionalized tissue-engineering scaffolds. *Journal of Biomedial Materials Research Part B Applied Biomaterials* 75 (2): 414–424.

78 Kolan, K.C.R., Leu, M.C., Hilmas, G.E., and Velez, M. (2012). Effect of material, process parameters, and simulated body fluids on mechanical properties of 13-93 bioactive glass porous constructs made by selective laser sintering. *Journal of the Mechanical Behavior of Biomedical Materials* 13 (Supplement C): 14–24.

79 Jain, P.K., Pandey, P.M., and Rao, P.V.M. (2008). Effect of delay time on part strength in selective laser sintering. *The International Journal of Advanced Manufacturing Technology* 43 (1): 117.

80 Gibson, I. and Shi, D. (1997). Material properties and fabrication parameters in selective laser sintering process. *Rapid Prototyping Journal* 3 (4): 129–136.

81 Gusarov, A.V., Laoui, T., Froyen, L., and Titov, V.I. (2003). Contact thermal conductivity of a powder bed in selective laser sintering. *International Journal of Heat and Mass Transfer* 46 (6): 1103–1109.

82 Dupin, S., Lame, O., Barrès, C., and Charmeau, J.-Y. (2012). Microstructural origin of physical and mechanical properties of polyamide 12 processed by laser sintering. *European Polymer Journal* 48 (9): 1611–1621.

83 Van der Schueren, B. and Kruth, J.P. (1995). Powder deposition in selective metal powder sintering. *Rapid Prototyping Journal* 1 (3): 23–31.

84 Leong, K.F., Chua, C.K., Gui, W.S., and V. (2006). Building porous biopolymeric microstructures for controlled drug delivery devices using selective laser sintering. *The International Journal of Advanced Manufacturing Technology* 31 (5): 483–489.

85 Berry, E., Brown, J.M., Connell, M. et al. Preliminary experience with medical applications of rapid prototyping by selective laser sintering. *Medical Engineering and Physics* 19 (1): 90–96.

86 Bourell, D.L., Watt, T.J., Leigh, D.K., and Fulcher, B. (2014). Performance limitations in polymer laser sintering. *Physics Procedia* 56 (Supplement C): 147–156.

87 Kruth, J.P., Levy, G., Klocke, F., and Childs, T.H.C. (2007). Consolidation phenomena in laser and powder-bed based layered manufacturing. *CIRP Annals* 56 (2): 730–759.

88 Yan, C., Shi, Y., and Hao, L. (2011). Investigation into the differences in the selective laser sintering between amorphous and semi-crystalline polymers. *International Polymer Processing* 26 (4): 416–423.

89 Williams, J.M., Adewunmi, A., Schek, R.M. et al. (2005). Bone tissue engineering using polycaprolactone scaffolds fabricated via selective laser sintering. *Biomaterials* 26 (23): 4817–4827.
90 Hao, L., Savalani, M.M., Zhang, Y. et al. (2006). Selective laser sintering of hydroxyapatite reinforced polyethylene composites for bioactive implants and tissue scaffold development. *Proceedings of the Institution of Mechanical Engineers, Part H: Journal of Engineering in Medicine* 220 (4): 521–531.
91 Tan, K.H., Chua, C.K., Leong, K.F. et al. (2005). Selective laser sintering of biocompatible polymers for applications in tissue engineering. *Biomedical Materials and Engineering* 15 (1–2): 113–124.